nature communications

Article

https://doi.org/10.1038/s41467-025-63613-w

Optimized in vivo base editing restores auditory function in a DFNA15 mouse model

Received: 21 November 2024

Accepted: 25 August 2025

Published online: 18 September 2025

Check for updates

Man Wang[1,2,10], Ziyu Zhang[1,10], Xiaohan Wang[1,10], Liyan Zhang[1,10], Xiangyan Chen[1], Nianci Li[1], Qiuhan Sun[1], Yicheng Lu[1], Zuhong He[1,3], Hongbo Yang[4] ✉, Fangzhi Tan[1] ✉, Jieyu Qi[5,6,7] ✉ & Renjie Chai[1,2,5,8,9] ✉

Genetic mutations cause hereditary deafness, in which mutations in the POU4 transcription factor 3 gene (*POU4F3*) lead to autosomal dominant non-syndromic deafness 15 (DFNA15), for which no effective clinical treatment currently exists. Gene editing holds promise for precisely repairing mutated nucleotides, thus offering a potential cure for hereditary hearing loss. Here, we establish a *Pou4f3*$^{WT/Q113*}$ mutant mouse model mimicking DFNA15. We develop and screen adenine base editors (ABEs) targeting the *Pou4f3*^{Q113*} allele by fusing diverse adenine deaminases to Cas9 we discovered before. SchABE8e accomplishes highly precise and efficient editing (up to 48.5%) at sgRNA3 in vitro. Neonatal *Pou4f3*$^{WT/Q113*}$ mice are treated via synthetic AAV (Anc80L65)-delivered SchABE8e-sgRNA3, resulting in near-complete hearing recovery, with the effect persisting for at least four months. Biosafety analyses further support the feasibility of base editing, providing a therapeutic strategy for DFNA15.

Hearing loss is a highly prevalent disease, affecting approximately 430 million people worldwide, accounting for about 5% of the global population[1]. Genetic deficiencies play a crucial role in the pathogenesis of deafness. Hearing loss can be classified as syndromic or non-syndromic based on the presence of accompanying symptoms in organs other than the inner ear. Approximately 80% of genetic deafness involves non-syndromic hearing loss (NSHL), which is further subdivided into autosomal recessive, autosomal dominant, X-linked, or mitochondrial deafness[2,3]. Over 50 causative genes have been identified for autosomal dominant NSHL (ADNSHL), including *POU4F3*[4].

Mutations in *POU4F3* have been confirmed as causative for DFNA15, with multiple mutations mapped to 5q31–33[5–8]. POU4F3 is a POU-type transcription factor that is exclusively expressed in the cochlea and vestibule of the inner ear. Previous studies had found that during cochlear development, the expression of POU4F3 remained high in both inner and outer hair cells (IHCs and OHCs) of adult mice. *Pou4f3* knockout causes severe hearing and balance disorders in mice, suggesting its crucial role in hair cell function[9–11]. DFNA15, a rare ADNSHL accounting for less than 1% of ADNSHL cases, had been genetically confirmed in limited pedigrees worldwide (e.g., in the Netherlands, China, Israel, and South Korea)[6,8,12–14]. Chinese cohorts

[1]Department of Otolaryngology Head and Neck Surgery, Zhongda Hospital, State Key Laboratory of Digital Medical Engineering, Jiangsu Provincial Key Laboratory of Critical Care Medicine, School of Life Sciences and Technology, School of Medicine, Advanced Institute for Life and Health, Southeast University, Nanjing, China. [2]Co-Innovation Center of Neuroregeneration, Nantong University, Nantong, China. [3]Department of Otorhinolaryngology-Head and Neck Surgery, Zhongnan Hospital of Wuhan University, Wuhan, China. [4]Obstetrics and Gynecology Hospital, Institute of Reproduction and Development, Fudan University, Shanghai, China. [5]Department of Radiology, Zhuhai People's Hospital, The Affiliated Hospital of Beijing Institute of Technology, Advanced Technology Research Institute, School of Life Science, Beijing Institute of Technology, Beijing, China. [6]State Key Laboratory of Hearing and Balance Science, Beijing Institute of Technology, Beijing, China. [7]Advanced Technology Research Institute, Beijing Institute of Technology, Jinan, China. [8]Department of Otolaryngology Head and Neck Surgery, Sichuan Provincial People's Hospital, School of Medicine, University of Electronic Science and Technology of China, Chengdu, China. [9]Southeast University Shenzhen Research Institute, Shenzhen, China. [10]These authors contributed equally: Man Wang, Ziyu Zhang, Xiaohan Wang, Liyan Zhang. ✉e-mail: hongboyang@fudan.edu.cn; tanfangzhi@163.com; qijieyu@bit.edu.cn; renjiec@seu.edu.cn

predominantly carry the *POU4F3* c.337C > T mutation, which clinically presents as adult-onset (20–40 years), bilateral, progressive, sensorineural hearing loss with pronounced high-frequency impairment[13]. This phenotype reflects POU4F3's essential role in hair cell maintenance, underscoring the need for population-tailored diagnostic and therapeutic strategies. However, there are currently no effective or preventive approaches for DFNA15.

Recently, the rapid developments in gene editing technologies have shown great promise for the research and clinical treatment of genetic diseases[15]. Gene therapy includes gene replacement, gene inhibition, and gene editing. Gene replacement therapy has been demonstrated to have significant therapeutic effects for autosomal recessive deafness and haploinsufficiency autosomal dominant deafness in mice[16], even in humans[17–19]. Gene editing enables precise targeted corrections and holds substantial potential for the clinical treatment of hereditary hearing loss[20,21]. In 2020, Yeh et al. used adeno-associated virus (AAV) to deliver a cytosine base editor (AID-CBEmax) into *Tmc*$^{Y182C/Y182C}$ mice, achieving effective hearing restoration and initiating the application of base editing for hereditary hearing loss[20]. Subsequently, in 2023, Peters et al. tested ABEs in *Pcdh15*^{R245X}, *Myo15-Cre+* mice and achieved partial hearing restoration[21], further demonstrating the potential of base editors in the treatment of hereditary hearing loss. However, precise gene editing methods for DFNA15 treatment have not yet been developed.

The pathogenic Q113* mutation results from a cytosine (C)-to-thymine (T) substitution in exon 2 of *POU4F3*, leading to a premature stop codon at amino acid position 113[13]. Currently, there are no base editing tools with high efficiency and safety that can make a T-to-C transition. The first ABE was developed in 2017 by Gaudelli et al.[22] and could convert adenine (A) to guanine (G) (equivalent to a T-to-C change on the complementary strand) in situ. It has since been continuously optimized for safety and efficiency. ABEs mainly consist of a Cas9 nickase (nCas9) and an engineered tRNA adenosine deaminase (enTadA). Using a single guide RNA (sgRNA), nCas9 recognizes the protospacer adjacent motif (PAM), binds to and unwinds double-stranded DNA. EnTadA deaminates A on the non-target strand to inosine, which is recognized as G during DNA replication, achieving an A•T to G•C base pair change[22]. In our previous study, we identified three Cas9 variants with simple PAMs and high activity, including SchCas9 (1054 amino acids, NNGR PAM, R = A or G), SpeCas9 (1058 amino acids, NNGG PAM), and Sha2Cas9 (1058 amino acids, NNGG PAM)[23,24]. These variants are approximately 300 amino acids smaller than the commonly used SpCas9 (1368 amino acids, NGG PAM), with comparable cleavage activity to SpCas9 and a similar PAM targeting range, indicating their therapeutic potential in the treatment of hereditary diseases.

The most commonly used adenine deaminase is TadA-8e, developed by Richter et al. in 2020 through phage-assisted continuous and non-continuous evolution of TadA7.10, resulting in a 590-fold activity increase. However, its wide editing window, bystander editing, and off-target activity pose safety risks[25]. Subsequently, Jeong et al. and Chen et al. developed more precise and safer TadA variants (TadA-8e-N108Q and TadA-8e-N108Q/L145T), which improved editing precision by several hundred-fold while moderately reducing deamination activity[26,27]. Integration of these improved Cas9 variants with adenosine deaminases may enable efficient and precise hearing restoration in *Pou4f3*^{Q113*} dominant deafness mice.

Based on these findings, we evaluate the therapeutic efficacy of our gene editing approach in *Pou4f3*$^{WT/Q113*}$ mice. This model exhibits progressive hair cell degeneration and postnatal hearing loss, effectively recapitulating the clinical phenotype of DFNA15 patients. Next, we establish a stable HEK293T cell line carrying the *Pou4f3*^{Q113*} mutant allele (HEK293T-*Pou4f3*^{Q113*} cell line) to test the editing efficiency of various combinations of nine ABEs and three sgRNAs. SchABE8e coupled with sgRNA3 demonstrates high editing efficiency and precision, as analyzed by BE-Analyzer[28]. To enhance in vivo therapeutic efficacy, we develop a split intein-mediated near-full-length protein reconstitution system. The dual AAV-SchABE8e-sgRNA3 system achieves an editing efficiency of 14.2 ± 2.5% in neonatal mouse cochleae, peaking at 30.4% efficiency at the complementary DNA (cDNA) level. Hearing in *Pou4f3*$^{WT/Q113*}$ mice is significantly restored, especially at low frequencies (nearly to normal levels). Biosafety studies in wild-type (WT) C57BL/6J mice, including auditory brainstem response (ABR) tests, hair cell morphological and quantitative analyses, vestibular function assessments, and body weight monitoring, demonstrate no adverse effects on behavior or normal hearing function. Together, our results lay the foundation for the clinical treatment of DFNA15.

Results

Establishment of *Pou4f3*^{Q113*} point mutant mice

POU4F3^{Q113*} (c.337C > T) in a Chinese family with DFNA15 deafness is caused by a C•G-to-T•A mutation in exon 2, which generates a truncated protein lacking the nuclear localization signal (NLS). Consequently, the mutant protein fails to localize to the nucleus, impairing its transcriptional regulatory function and ultimately causing hair cell dysfunction and hearing loss[13]. The *POU4F3* sequence is highly conserved among vertebrates, including rodents and humans (Fig. 1A). We constructed the corresponding non-humanized mouse model carrying the *Pou4f3*^{Q113*} mutation to simulate DFNA15. Sanger sequencing confirmed successful establishment of the *Pou4f3*^{Q113*} mouse line (Fig. 1B). ABR recordings, including click ABR and tone-burst ABR (TB-ABR), were performed to assess age-dependent hearing threshold changes in mice. We found that the *Pou4f3*$^{WT/Q113*}$ mice exhibited normal hearing at postnatal day 30 (P30) compared to WT controls, but showed progressive hearing loss thereafter (Fig. 1C, D). To delineate the progression of OHC pathology, we longitudinally assessed auditory function in heterozygous and WT mice from 1 to 3 months using distortion product otoacoustic emissions (DPOAEs), which revealed early-onset OHC dysfunction. *Pou4f3*$^{WT/Q113*}$ mice showed significant amplitude reductions at P30, preceding detectable threshold shifts in ABRs (Supplementary Fig. 1A). The functional impairment progressed in an age-dependent manner, culminating in pronounced OHC loss predominantly in the middle and basal turns at 3 months. Consistent with DPOAE findings, immunostaining at 3 months confirmed substantial OHC degeneration in *Pou4f3*$^{WT/Q113*}$ mice, with the middle and basal regions most severely affected (Fig. 1E, F).

Complementary ultrastructural analysis via scanning electron microscopy (SEM) revealed alterations in stereocilia bundle morphology in the OHC regions of *Pou4f3*$^{WT/Q113*}$ cochleae (Fig. 1G). These SEM findings correlated precisely with immunofluorescence-based quantification of hair cell loss, demonstrating consistent OHC pathology across both nanometer-scale (SEM) and micrometer-scale (light microscopy) resolutions. The concordance between these independent methodological approaches strengthens the validity of our conclusions regarding *Pou4f3*-dependent stereocilia maintenance. We also verified that the biallelic *Pou4f3*$^{Q113*/Q113*}$ mutation exhibited profound hearing loss with complete hair cell degeneration and cochlear structural collapse at P30 (Supplementary Fig. 1B–D), presenting a more severe phenotype than typically observed in DFNA15 patients.

Optimization of ABEs targeting the *Pou4f3*^{Q113*} mutation site

The pathogenic mutation Q113* results from a C-to-T conversion at position 113 in exon 2 of murine *Pou4f3*. Consequently, an ABE capable of mediating an A•T to G•C conversion on the antisense strand was required[22]. Here, we generated nine ABEs by combining three high-activity Cas9 variants (SchCas9, SpeCas9, and Sha2Cas9) with simple PAMs that we developed previously[23,24] and three adenosine deaminase versions (TadA-8e, TadA-8e-N108Q, and TadA-8e-N108Q/L145T)

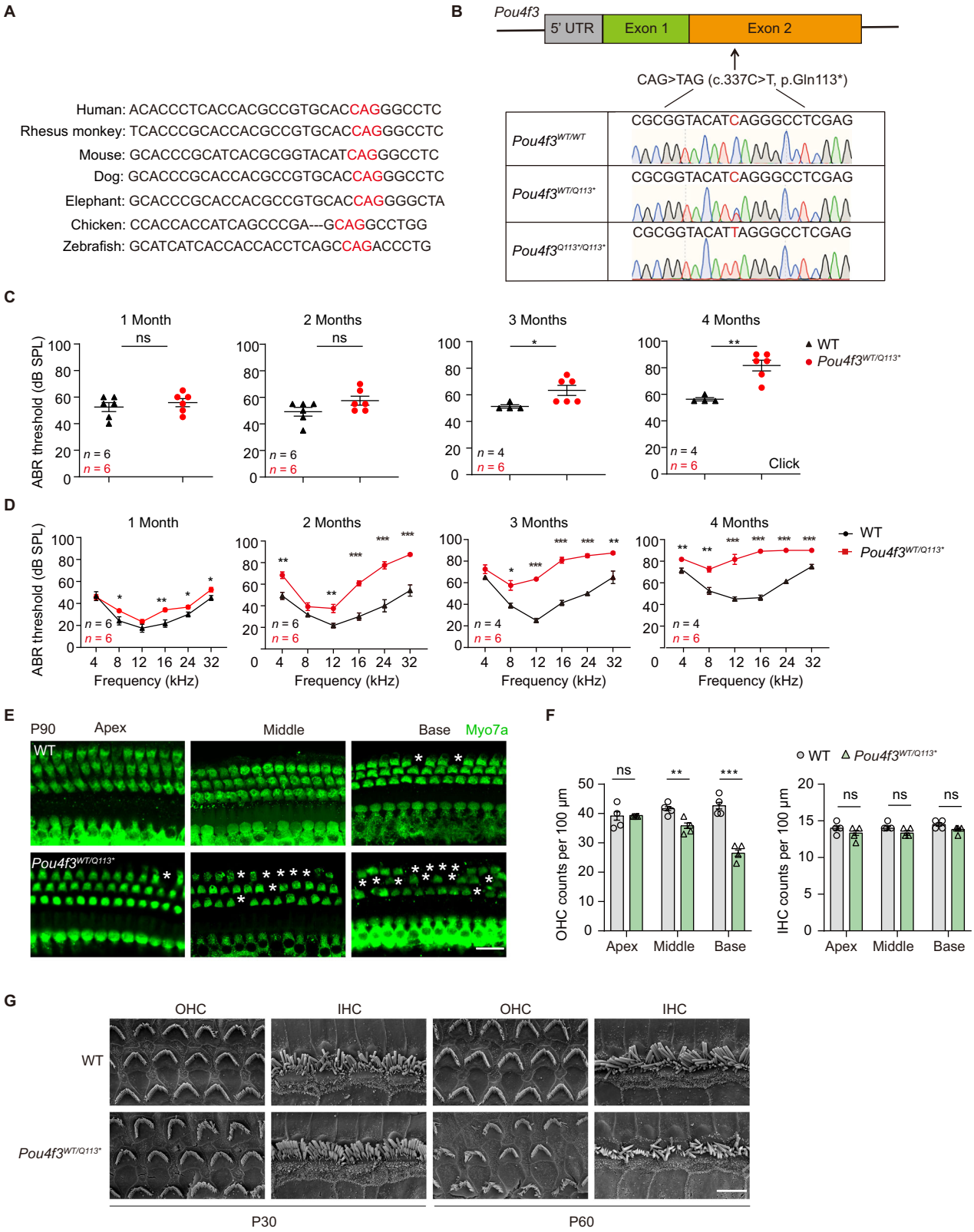

(Fig. 2A). In addition, three target sites (sgRNA1, sgRNA2, and sgRNA3) were designed by screening for the PAM, the location within the editing window, and the predicted off-target potential (Fig. 2B). ABEs and sgRNAs were screened in the HEK293T-*Pou4f3*^{Q113*} cell line. The commonly used ABE8e, along with two sgRNAs (sgRNA4 and sgRNA5), served as controls to benchmark the effectiveness and safety of our ABEs at the target locus (Fig. 2B).

For the ABE8e tools, Sha2ABE8e-sgRNA1/2 and SpeABE8e-sgRNA1/2 showed high on-target activity (58.6–74.5%) but also displayed substantial off-target A-to-G conversions at neighboring adenines (13–79.4%), while SchABE8e-sgRNA3 achieved moderate activity (~48.5%) with lower bystander editing (~6.2%). The ABE8e-N108Q tools (SchABE8e-N108Q, SpeABE8e-N108Q, Sha2ABE8e-N108Q) and ABE9 tools (SchABE9, SpeABE9, Sha2ABE9) generally showed lower editing

https://doi.org/10.1038/s41467-025-63613-w

Fig. 1 | Establishment of *Pou4f3*$^{WT/Q113*}$ transgenic mice. A The amino acid substitution in *Pou4f3* (c.337C > T, p.Q113*) mutant mice occurs at a location (red) that is highly conserved in vertebrate evolutionary clades such as humans, monkeys, and zebrafish. **B** Representative Sanger sequencing results of the *Pou4f3 allele* in WT, *Pou4f3*$^{WT/Q113*}$ and *Pou4f3*$^{Q113*/Q113*}$ mice. **C** The results of click ABR thresholds in *Pou4f3*$^{WT/Q113*}$ mice (red) and WT mice (black). WT vs *Pou4f3*$^{WT/Q113*}$: $p = 0.476179$ (1 month), $p = 0.105612$ (2 months), $p = 0.037513$ (3 months), $p = 0.001093$ (4 months). **D** The results of TB-ABR thresholds in *Pou4f3*$^{WT/Q113*}$ mice (red) and WT mice (black). (WT vs *Pou4f3*$^{WT/Q113*}$: 1 month, $p = 0.861927$ (4k), $p = 0.040231$ (8k), $p = 0.191765$ (12k), $p = 0.006708$ (16k), $p = 0.037929$ (24k), $p = 0.035894$ (32k); 2 months, $p = 0.001634$ (4k), $p = 0.082764$ (8k), $p = 0.004614$ (12k), $p = 0.000023$ (16k), $p = 0.000192$ (24k), $p = 0.000097$ (32k); 3 months, $p = 0.174963$ (4k), $p = 0.012478$ (8k), $p < 0.000001$ (12k), $p = 0.000007$ (16k), $p < 0.000001$ (24k), $p = 0.001515$ (32k); 4 months, $p = 0.001956$ (4k), $p = 0.001110$ (8k), $p = 0.000275$ (12k), $p < 0.000001$ (16k), $p < 0.000001$ (24k), $p = 0.000015$ (32k). **E** Representative immunofluorescence images of hair cells from WT and the *Pou4f3*$^{WT/Q113*}$ mice at P90, $n = 4$ independent experiments with similar results. Myo7a (green): hair cell marker. '*' Indicates the missing hair cells. Scale bar, 20 μm. **F** Quantification of cochlear hair cells corresponding to (**F**). $n = 4$, WT vs *Pou4f3*$^{WT/Q113*}$: in OHCs, $p > 0.999999$ (apex), $p = 0.002452$ (middle), $p = 0.000050$ (base), in IHCs, $p = 0.113532$ (apex), $p = 0.097160$ (middle), $p = 0.097160$ (base). **G** Representative SEM micrographs of OHCs and IHCs in the cochleae from WT and *Pou4f3*$^{WT/Q113*}$ mice at P30 and P60, $n = 3$ independent experiments with similar results. Scale bar, 5 μm. Data in (**C**, **D**, **F**) are represented as mean ± SEM. Statistical significance was determined by unpaired two-tailed Student's *t*-tests ($^{*}p < 0.05$, $^{**}p < 0.01$, $^{***}p < 0.001$, ns no significant difference). Source data are provided as a Source data file.

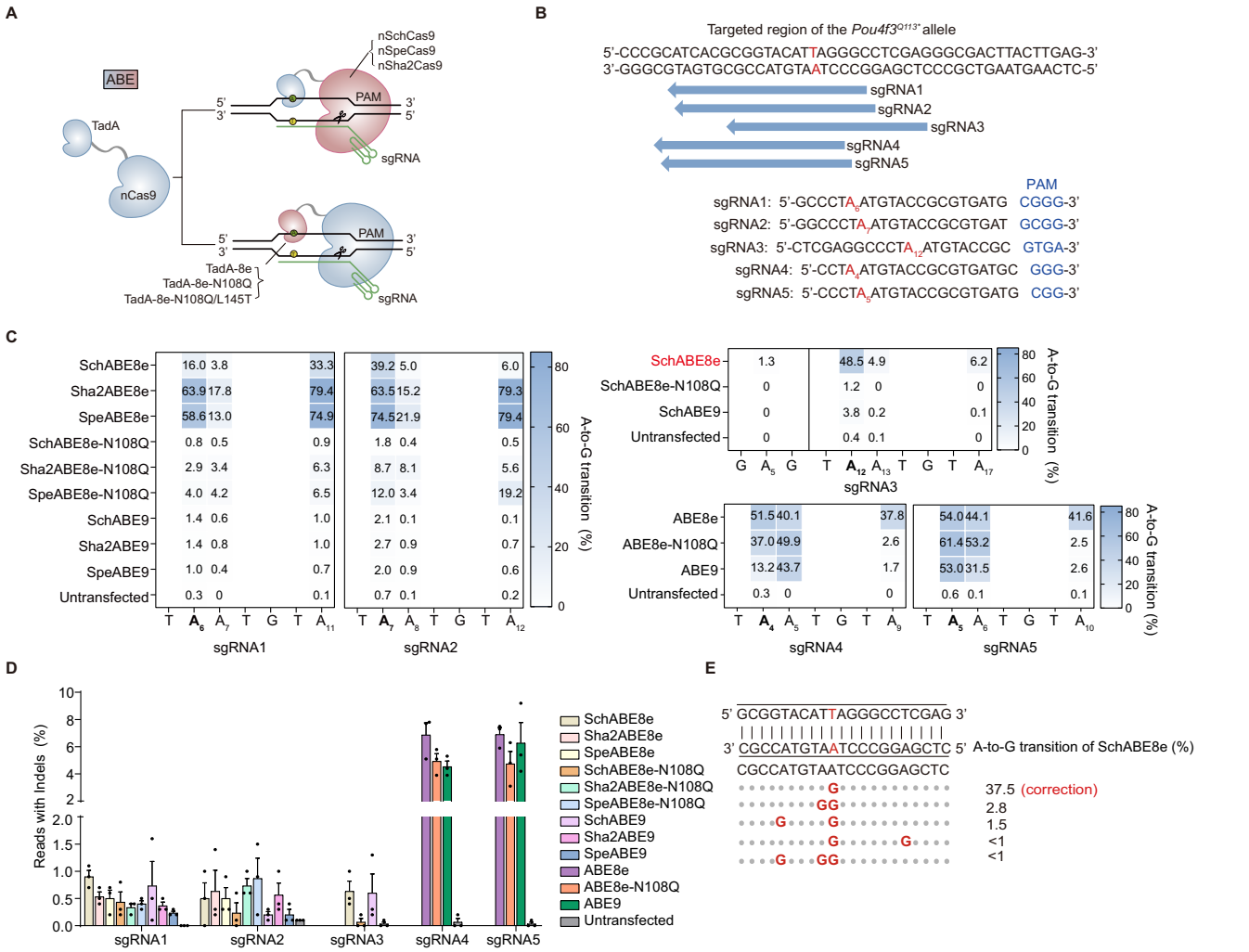

Fig. 2 | Construction of ABEs targeting the *Pou4f3*^{Q113*} mutation site. A Structural diagram of the ABE base editors, consisting of TadA deaminase and nCas9. The red color represents the subunit that varied, with nCas9 (above) as the variable, and TadA (below) as the variable. The sgRNA is in green, and the dsDNA is in black. A·T is the target base pair. **B** Schematic of the *Pou4f3* locus highlighting the c.337C > T mutation and the five candidate sgRNAs that the position of target A (in red) in the protospacer (6, 7, 12, 4, and 5) and that use different PAMs (CGGG, GCGG, GTGA, GGG, and CGG, in blue). **C** The heat maps represent the A-to-G transition frequency of the 12 ABEs at five targets (sgRNA1-5) in the HEK293T-*Pou4f3*^{Q113*} cell lines. Data were collected from three independent experiments. **D** The frequencies of indel formation by twelve ABEs at five target sites in (**A**, **B**), corresponding to NGS data analysis. Data are represented as mean ± SEM from three independent experiments. **E** The precision of A-to-G base editing at the sgRNA3 by SchABE8e. A-to-G (red); "correction": no bystanders. Source data are provided as a Source data file.

efficiencies (~12%). The control ABE8e efficiently edited sgRNA4/5 but also induced high off-target activity at adjacent adenines, causing significant bystander editing (~50%) (Fig. 2C). Altogether, SchABE8e combined with sgRNA3 demonstrated a favorable balance of moderate on-target editing efficiency and minimal bystander activity.

Next, we further evaluated SchABE8e-sgRNA3 for safety and precision. Base editors use a nCas9 to induce single-strand nicks rather than double-strand breaks. By nicking only the non-edited strand, they promote DNA repair mechanisms that enable precise base editing while greatly reducing unwanted indel formation—although rare indels

may still occur, they are substantially less frequent than with traditional Cas9-mediated cleavage[29]. Indel frequencies in the HEK293T-*Pou4f3*^{Q113*} cell line were lower for our nine ABEs compared to the ABE8e toolbox, especially for SchABE8e (<1% indels), indicating enhanced safety (Fig. 2D). Given that bystander editing may undermine in vivo therapeutic efficacy, we undertook a thorough analysis of editing precision. Specifically, we conducted a detailed analysis using a set of SchABE8e-sgRNA3. The next-generation sequencing (NGS) analysis, performed using BE-Analyzer, showed a base editing efficiency of 45.9% at position A12. Critically, 37.5% of the edits were precise, with no bystander editing, demonstrating high editing precision (Fig. 2E). These data demonstrate—from multiple perspectives including editing activity, bystander editing, safety, and precision—that SchABE8e-sgRNA3 is the most promising candidate for gene therapy in *Pou4f3*$^{WT/Q113*}$ mice.

To better simulate the in vivo editing efficiency observed in DFNA15 patients, we tested the editing potential of SchABE8e for the human mutation (*POU4F3*, 337C > T) using a humanized cell model. We integrated the exon 2 sequence carrying the c.337C > T mutation of human *POU4F3* into HEK293T cells via lentiviral delivery to generate a stable mutated cell line. Due to the presence of the wild-type *POU4F3* exon 2 sequence in the genome, we detected about 15–18% G at this mutation site (Supplementary Fig. 2B). Based on the NNGR PAM of SchABE8e, the location within the editing window, and the predicted off-target potential, we designed another four sgRNAs that target the human *POU4F3*^{Q113*} site (Supplementary Fig. 2A). After transfecting of SchABE8e with these sgRNAs, sgRNA4 showed the highest efficiency at 31.8% (background-corrected by subtracting the 17% baseline G content), with negligible bystander editing (Supplementary Fig. 2B). Furthermore, potential off-target sites (OT1–7) for sgRNA4 were predicted using Benchling, with negligible off-target activity (near-zero background; Supplementary Fig. 2C).

Considering the comparable editing efficiencies observed at the homologous mutation sites in mouse and human HEK293T cells, SchABE8e demonstrates therapeutic potential for treating DFNA15 patients harboring the *POU4F3* c.C337T variant.

Characterization and optimization of SchABE8e

To explore the clinical applicability of SchABE8e, we characterized its activity at 12 endogenous targets. The editor achieved efficiencies of 2–40% at 7 of 12 targets (Supplementary Fig. 3A). A systematic analysis revealed an effective editing window spanning protospacer positions 6–14 (Supplementary Fig. 3B), demonstrating broad applicability across genomic contexts. NGS analysis of SchABE8e editing outcomes revealed predominant A-to-G transition, with minimal T/C byproducts (Supplementary Fig. 3C). Indel frequencies at all seven endogenous targets revealed consistently low rates (<1%) (Supplementary Fig. 3D), thus providing evidence for the safety profile of SchABE8e.

Off-target activities pose a significant challenge to the transition of gene editing from fundamental research to clinical applications. DNA off-target activity is primarily categorized into Cas9-dependent and Cas9-independent off-targets[30,31]. Cas9-dependent off-targets arise from the non-specific binding of Cas9 to genomic sites with high sequence similarity. To evaluate Cas9-dependent off-target effects, we designed 9 mismatch sites (OT1–9, ≤4 mismatches) against the efficient endogenous target (target 1). Notably, NGS revealed negligible editing at these sites in HEK293T cells, highlighting SchABE8e's high specificity (Supplementary Fig. 3E). Conversely, Cas9-independent off-targets are primarily attributed to deaminase activity. The TadA-8e deaminase has been demonstrated to have potential Cas9-independent off-target activity[25]. Since the off-target activity might vary with different nCas9, we employed an orthogonal R-loop assay to detect the Cas9-independent off-target DNA editing of SchABE8e sensitively[31]. Given the homology between SchCas9 and SaCas9—which shares the same gRNA scaffold[24]—we custom-designed dSpCas9/SpsgRNA R-loop complexes for assessment (Supplementary Fig. 3F). HEK293T cells were co-transfected with plasmids encoding SchABE8e plus its on-target sgRNA, along with dSpCas9 and an off-target SpCas9 sgRNA (targeting an unrelated locus). This assay revealed high A•T-to-G•C conversion efficiencies at target 1 (Supplementary Fig. 3G), while the off-target editing was ~6% at Sp site 1 vs ≤1% at five dSpCas9 R-loop off-target sites (Supplementary Fig. 3H). The minimal editing at five SpCas9 targets confirms SchABE8e's low Cas9-independent off-target activity. Therefore, these findings show that SchABE8e exhibits a broad editing window, high precision, and low levels of byproducts/off-target activity, suggesting its translational potential for in vivo therapeutic applications.

To enhance editing efficiency of SchABE8e, we engineered two SchABE8e variants: eeSchABE8e (HMG-D double-strand DNA-binding domain[32] fused to nSchCas9's C-terminus) and hySchABE8e (Rad51 single-strand DNA-binding domain[33] fused to nSchCas9's N-terminus) (Supplementary Fig. 4A). Evaluation at the sgRNA3 site showed moderate improvement but increased bystander editing and indel frequencies (Supplementary Fig. 4B, C). Given safety for gene therapy, we used SchABE8e to treat *Pou4f3*$^{WT/Q113*}$ mice.

Treatment strategies for AAV-SchABE8e-sgRNA3

The efficacy of gene therapy relies on the efficiency of the base editor, as well as the transduction/expression capability of AAV[34–36]. Given that the POU4F3 protein is predominantly expressed in cochlear hair cells, we selected Anc80L65 for treating *Pou4f3*$^{WT/Q113*}$ mice due to its high efficiency at transducing hair cells[37,38]. The WPRE element (~600 bp) has been reported to enhance transgene expression[39]. Prior to therapeutic application, we first assessed the effect of the WPRE element on transgene expression in the cochlea. Two AAV-EGFP constructs, one with WPRE (AAV-CMV-EGFP-WPRE-SV40PolyA) and one without (AAV-CMV-EGFP-SV40PolyA), were packaged into Anc80L65 capsid. Following round-window membrane injection (4.5×10^{10} genome copies (GCs)) in P1–3 WT mice, immunofluorescence at 2 weeks post-injection revealed markedly weaker transduction without WPRE (Fig. 3A, B), demonstrating that WPRE critically enhances transgene expression in the cochlear hair cells. Since the therapeutic base editor carrying the WPRE, along with other essential elements, exceeds the packaging capacity of AAV, it is necessary to split SchABE8e into two fragments for dual AAV packaging.

Self-cleaving inteins autonomously excise from precursor proteins while simultaneously ligating flanking polypeptides[40]. We employed a split-intein system to facilitate *trans*-splicing-mediated protein recombination to form the full-length SchABE8e. Five split sites of SchABE8e were carefully selected to ensure that they did not compromise the integrity of important secondary structures and that they were situated within non-essential amino acid sequences in the protein's secondary structure. These split-SchABE8e variants were constructed into two corresponding AAV vectors. Western blot analysis validated the recombination efficiency of SchABE8e variants in HEK293T cells, revealing differential protein reconstitution efficiencies among Split-SchABE8e variants 1, 2, 4, and 5 (Fig. 3C). Quantification analysis revealed that variants 2 and 4 achieved expression levels comparable to full-length SchABE8e, with variant 4 exhibiting superior reconstitution efficiency (Fig. 3D). Furthermore, the gene editing efficiency also showed that split-SchABE8e variant 4-sgRNA3 had the highest editing efficiency (41%), which is comparable to the full-length SchABE8e (Fig. 3E). Based on comprehensive evaluation of protein expression and editing efficiency, split-SchABE8e variant 4 was selected for gene therapy.

In vivo editing efficiency and off-target analysis of SchABE8e

We delivered a 1:1 GC ratio mixture of the two therapeutic AAVs (total dose: 4.5×10^{10} GCs/ear; 3×10^{13} GC/mL in 1.5 µL) via round-window membrane injection into the cochleae of P1–3 *Pou4f3*$^{WT/Q113*}$ neonatal

https://doi.org/10.1038/s41467-025-63613-w

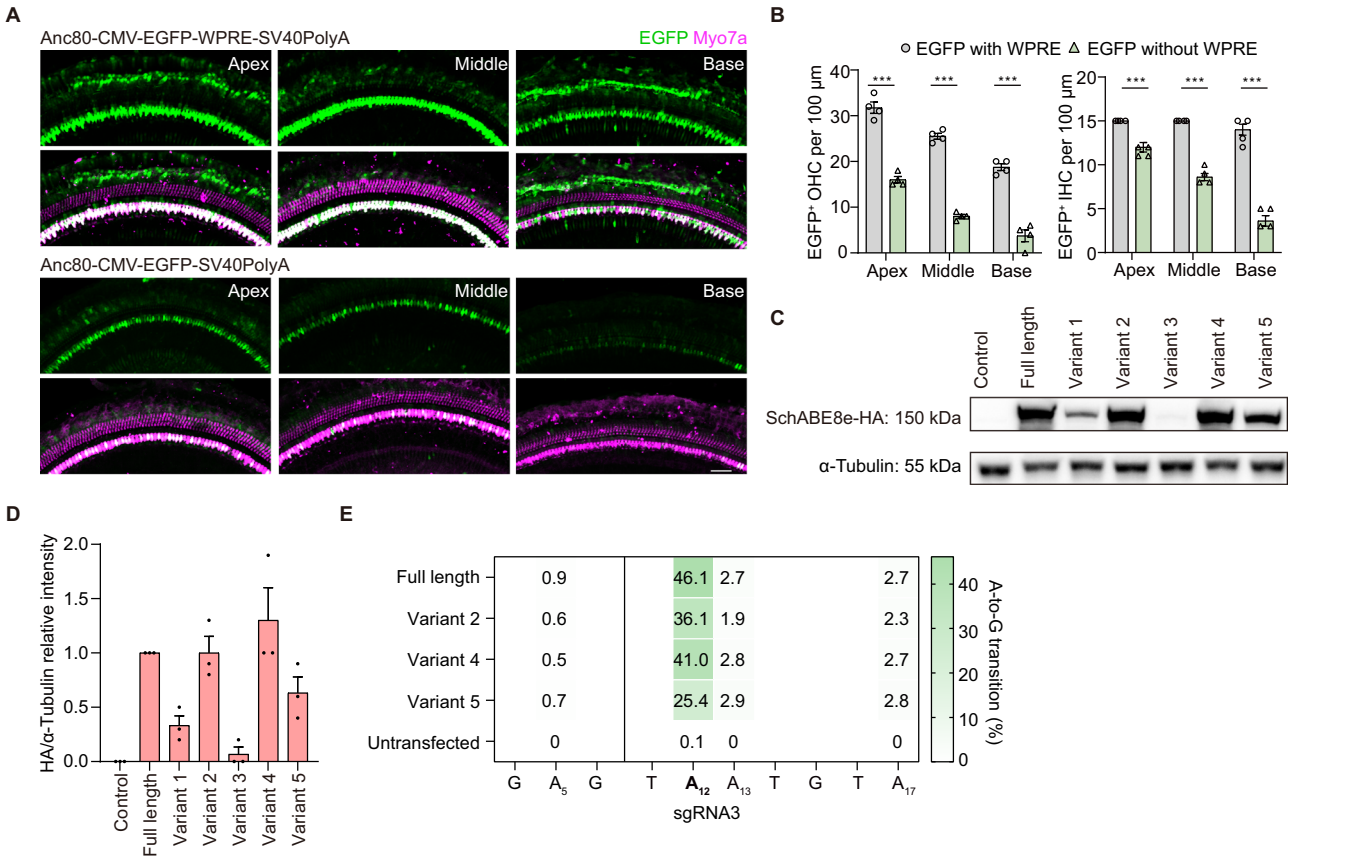

Fig. 3 | Evaluating the impact of WPRE on transgene expression mediated by Anc80L65. A Whole-mount preparations of the cochlea showing the distribution of EGFP fluorescent protein in hair cells after AAV injection into the P1–3 mouse cochlea, $n = 4$ independent experiments with similar results. Myo7a (purple): hair cell marker. Scale bar, 50 μm. **B** The number of EGFP-positive OHCs (left) and IHCs (right) per 100 μm length, $n = 4$. WT vs *Pou4f3*$^{WT/Q113*}$: in OHCs, $p = 0.000034$ (apex), $p < 0.000001$(middle), $p = 0.000061$ (base), in IHCs, $p = 0.000019$ (apex), $p = 0.000012$ (middle), $p = 0.000049$ (base). **C**, **D** Split-site screening of split-SchABE8e. **C** Western blotting results of the intein-mediated recombination expression of the five split-SchABE8e variants. **D** Quantitative analysis of SchABE8e expression by calculating the grayscale intensity of the HA tag from three independent experiments using ImageJ software (Fiji, Inc.). **E** Heatmap of editing efficiency of the split-SchABE8e variants with sgRNA3. Data were collected from three independent experiments. Data in (**B**, **D**) are represented as mean ± SEM. Statistical significance was determined by unpaired two-tailed Student's *t*-tests (***$p < 0.001$). Source data are provided as a Source data file.

mice (Fig. 4A). One week post-injection, in vivo NGS analyses of editing efficiency at the pathogenic site were conducted at both genomic DNA and cDNA levels (Fig. 4B). The DNA editing results demonstrated a statistically difference in the G/(A + G) ratio between injected ears and both contralateral ears or uninjected controls. The mean editing efficiency was 3.8 ± 0.9% (mean ± SEM), with peaking efficiency reaching 8.9% (Fig. 4B). Analysis of cDNA editing also revealed significant differences: injected ears exhibited a higher G/(A + G) ratio compared to contralateral ears and uninjected controls. Specifically, there was a marked distinction between injected and contralateral ears. The editing efficiency at the cDNA level was 14.2 ± 2.5% (mean ± SEM), with the highest efficiency reaching 30.4% (Fig. 4B). From both the genomic DNA and the cDNA perspectives, the comprehensive analysis reveals that dual AAV-SchABE8e-sgRNA3 effectively corrected the *Pou4f3* (c.337C > T) allele.

To evaluate the off-target effects of SchABE8e-sgRNA3 in mice, we first designed nine potential DNA off-target sites (OT1–9) with high sequence similarity to sgRNA3 using Benchling. Off-target editing analysis of the cochlear genome showed minimal impact (Fig. 4C).

For comprehensive off-target evaluation, we performed Whole Genome Sequencing (WGS) on pooled cochlear sensory epithelia from three treated ears (due to limited tissue availability), with age-matched untreated heterozygous mouse ears serving as controls. WGS results showed that the treated and the untreated groups had comparable frequencies of single-nucleotide variants (SNVs) and indels. Furthermore, no detectable off-target sites via Off-Finder analysis (mismatches ≤ 4; Table 1 and Supplementary Fig. 5A–D). Collectively, these results demonstrate minimal off-target activity, indicating that SchABE8e-sgRNA3 can precisely and effectively correct the pathogenic *Pou4f3* (c.337C > T) allele.

Precision base editing in vivo restored hearing in *Pou4f3*$^{WT/Q113*}$ mice

Dual AAV-SchABE8e-sgRNA3 was injected into the cochleae of P1–3 *Pou4f3*$^{WT/Q113*}$ mice via the round-window membrane. Hearing recovery was assessed by ABR at 2 months post-injection, with untreated *Pou4f3*$^{WT/Q113*}$ ears and the WT mice ears serving as controls. The average click ABR threshold of the treated ears was 60 decibels (dB) sound pressure levels (SPL) two months after treatment in the *Pou4f3*$^{WT/Q113*}$ mice, which was comparable to age-matched WT controls (60 dB SPL). The average threshold was 70 dB SPL in the untreated ears. Hearing recovery of *Pou4f3*$^{WT/Q113*}$ mice was stable for at least four months post-surgery (Fig. 4D). TB-ABR analysis showed that, compared to the untreated ears, the dual AAV-SchABE8e-sgRNA3 injected ears exhibited significantly improved auditory thresholds at the tested frequencies (4 kHz, 8 kHz, 12 kHz, and 16 kHz), achieving WT-equivalent thresholds at two months (Fig. 4E, F). Long-term follow-up over four months showed sustained hearing recovery at middle-to-low frequencies (4–12 kHz), with thresholds comparable to those of WT ears

https://doi.org/10.1038/s41467-025-63613-w

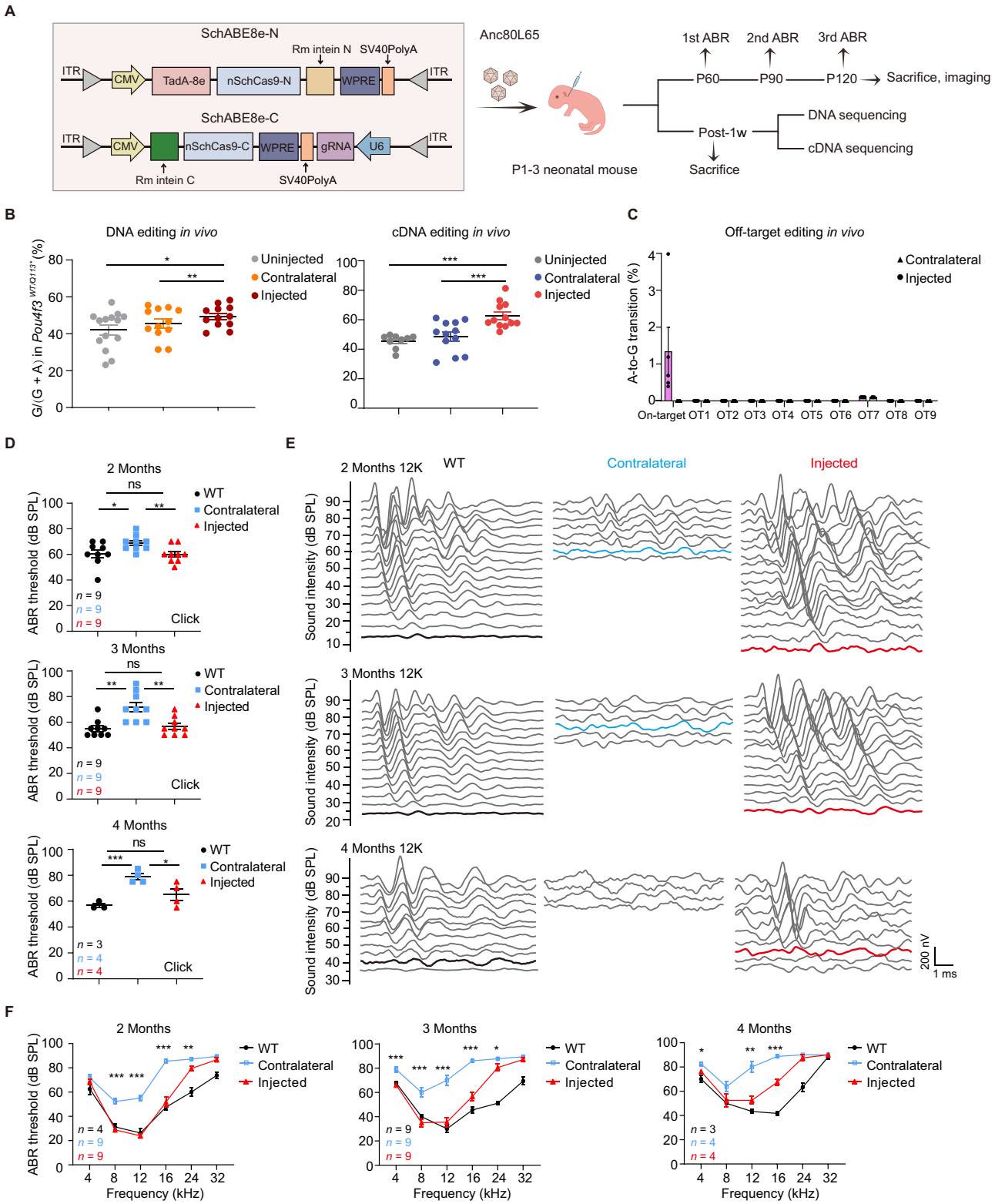

(Fig. 4F). Collectively, these results demonstrated that precise gene therapy enabled durable hearing restoration in *Pou4f3*$^{WT/Q113*}$ mice.

Therapy restored POU4F3 nuclear localization and enhanced hair cell survival in *Pou4f3*$^{WT/Q113*}$ mice

The c.337C > T mutation changes the glutamine codon (CAG) at position 113 of the POU4F3 protein to a stop codon (TAG), resulting in a truncated POU4F3 protein lacking NLS, which impairs the subcellular localization of the POU4F3 and prevents its nuclear entry[13]. Consistent with this, we detected the cytoplasmic POU4F3 protein surrounding the nucleus in the hair cells of *Pou4f3*$^{WT/Q113*}$ mice (Fig. 5A). To quantify the recovery of POU4F3 localization in cochlear hair cells post-treatment, we calculated the POU4F3-positive area to DAPI-positive nuclear area (POU4F3/DAPI area ratio) for each OHC and IHC. In treated *Pou4f3*$^{WT/Q113*}$ mice, both OHCs and IHCs in treated *Pou4f3*$^{WT/Q113*}$ mice demonstrated improvement compared to untreated ears (Fig. 5B).

To further assess tissue-level editing efficiency following gene therapy, we quantified the number of OHCs and IHCs with restored

Fig. 4 | Precision in vivo base editing effectively restores hearing in *Pou4f3*$^{WT/Q113*}$ mice. A Study design of the intein-mediated dual AAV-SchABE8e-sgRNA3 therapy. **B** G/(A + G) ratios in cochleae of uninjected (gray, $n = 14$), injected with dual AAV-SchABE8e-sgRNA3 (brown, $n = 12$), and contralateral ears (orange, $n = 12$) at 1 week post-injection in DNA level (left). Injected vs uninjected: $p = 0.2154$, injected vs contralateral: $p = 0.0011$. In the cDNA level (right), uninjected (gray, $n = 9$), injected with dual AAV-SchABE8e-sgRNA3 (red, $n = 12$), and contralateral ears (blue, $n = 12$) are shown. Injected vs uninjected: $p = 0.0001$, injected vs contralateral: $p = 0.0018$. **C** Off-target activity analysis of the nine candidate sites identified by Benchling in *Pou4f3*$^{WT/Q113*}$ treated mice after one week. The on-target sites and the top nine off-target sites (OTs) were analyzed by NGS. Data were collected from five independent experiments. **D**–**F** Click ABR (**D**) and TB-ABR (**E**, **F**) thresholds in WT (black) and *Pou4f3*$^{WT/Q113*}$ mice injected with AAV-SchABE8e-sgRNA3 (red) and contralateral ears (blue) at 2-, 3-, and 4-month post-injection. **D** Thresholds in injected ears (red) didn't differ significantly from age-matched WT controls (black) across time points. WT vs contralateral: $p = 0.039710$ (2 months), $p = 0.001418$ (3 months), $p = 0.000919$ (4 months); contralateral vs injected: $p = 0.008767$ (2 months), $p = 0.003647$ (3 months), $p = 0.037131$ (4 months); WT vs injected: $p = 0.862433$ (2 months), $p = 0.61264$ (3 months), $p = 0.195394$ (4 months). **E** ABR traces of 12 kHz. **F** TB-ABR thresholds. 2 months, contralateral vs injected: $p = 0.332195$ (4k), $p < 0.000001$ (8k), $p < 0.000001$ (12k), $p = 0.000002$ (16k), $p = 0.002180$ (24k), $p = 0.091392$ (32k); 3 months, contralateral vs injected: $p = 0.000731$ (4k), $p = 0.000171$ (8k), $p = 0.000010$ (12k), $p < 0.000001$ (16k), $p = 0.031688$ (24k), $p = 0.229491$ (32k); 4 months, contralateral vs injected: $p = 0.016965$ (4k), $p = 0.145704$ (8k), $p = 0.002659$ (12k), $p = 0.000270$ (16k), $p = 0.355918$ (24k). At 2 months post-injection, *Pou4f3*$^{WT/Q113*}$ mice injected with AAV-SchABE8e-sgRNA3 exhibited threshold improvements of 40 (8 kHz), 30 (12 kHz), and 40 dB SPL (16 kHz) compared to contralateral ears. Hearing recovery remained stable at 3–4 months in the middle- and low-frequency range (4–16 kHz), while hearing recovery in the high-frequency thresholds showed persistent elevation, with a residual deficit of ~25 dB SPL vs WT controls. Data in (**B**, **C**, **D**, **F**) are represented as mean ± SEM. Statistical significance was determined by unpaired two-tailed Student's *t*-tests, except for comparisons between injected and contralateral groups in (**B**), which were analyzed by paired two-tailed Student's *t*-tests ($^{*}p < 0.05$, $^{**}p < 0.01$, $^{***}p < 0.001$, ns no significant difference). Source data are provided as a Source data file.

Table 1 | Numbers of indels and SNVs detected by whole-genome sequencing

	Treated	Untreated
Raw indel/SNVs	315,607	310,623
Sample-specific indels (other filter)	26,571	25,880
Reads numbers > 2	26,009	25,354
On-target	1	1
Off-target sites	0	0

nuclear POU4F3 expression within 100 µm cochlear segments. We calculated the ratio of edited cells relative to the total number of corresponding hair cells, using the maximum POU4F3/DAPI area ratio in each turn of WT mice as the recovery threshold. The results indicate a significant restoration of nuclear POU4F3 expression in both OHCs and IHCs of treated *Pou4f3*$^{WT/Q113*}$ mice (Fig. 5C).

The *Pou4f3*$^{WT/Q113*}$ mice exhibited significant OHC degeneration in the middle and basal cochlear turns (Fig. 1E, F). To assess hair cell survival post-treatment, we immunostained and counted hair cells three months after AAV-SchABE8e-sgRNA3 injection. The number of OHCs in the treated ears (middle turn: 42 ± 1 cells/100 µm; basal turn: 38 ± 1 cells/100 µm) was higher than in the untreated ear (middle turn: 36 ± 1 cells/100 µm; basal turn: 25 ± 1 cells/100 µm), indicating improved OHC preservation after treatment (Fig. 5D, E).

The dual AAV-SchABE8e-sgRNA3 therapeutic strategy is safe for inner ear application

To evaluate the safety of this therapy, our study focused on evaluating its impact on the auditory and nervous system in WT mice following a single inner ear injection of dual AAV-SchABE8e-sgRNA3. Utilizing the same surgical route, an equivalent therapeutic dose of virus was administered into the inner ear of neonatal WT mice. ABR testing at 1-, 2-, and 3-month post-injection revealed no significant threshold difference across all frequencies between injected ears and WT controls (Fig. 6A). Three months post-injection, mice were euthanized, and the cochlear epithelial structure was examined. Immunofluorescence results showed no morphological changes in the sensory epithelium of the virus-injected ear (Fig. 6B). The number of hair cells showed no statistical difference compared to the untreated ear (Fig. 6C).

Given that Anc80L65 injection through the round window was also able to transduce vestibular hair cells, behavioral tests were conducted at P90 to rule out any potential toxicity of AAV-SchABE8e-sgRNA3 on the vestibular system. Results revealed no statistical differences between AAV-injected and uninjected WT mice in either rotarod performance or open field exploration (Fig. 6D), demonstrating that a therapeutic dose of dual AAV-SchABE8e-sgRNA3 did not cause motor or coordination deficits. Statistical analysis of body weight also showed no significant differences between AAV-injected and age-matched control mice at P30, P60, and P90 after AAV injection (Fig. 6E). Collectively, these results indicate that local inner ear injection of dual AAV-SchABE8e-sgRNA3 neither compromised the normal structure and physiological function of the inner ear nor exerted any adverse effects on the nervous system.

Therapeutic efficacy was limited in homozygous *Pou4f3*$^{Q113*/Q113*}$ mice

To further explore this, we administered 1.5 µL viral injections (4.5×10^{10} GCs) into the inner ear of neonatal *Pou4f3*$^{Q113*/Q113*}$ homozygous mice and evaluated their auditory function two months post-injection using click ABR and TB-ABR testing. Results reflected a lack of therapeutic effect (Supplementary Fig. 6A). Immunofluorescence analysis of cochleae from P3 and P7 homozygous mice revealed extensive hair cell loss prior to intervention (Supplementary Fig. 6B), implying that pre-existing cellular damage may underlie the lack of therapeutic response. This observation raises the possibility that the optimal therapeutic window for homozygous mice occurs earlier, potentially during the embryonic stage. Notably, homozygous mice also exhibited high neonatal mortality rates and significantly reduced body weight compared to age-matched WT and heterozygous mice (Supplementary Fig. 6C), further indicating inherent physiological compromise.

Discussion

Genetic factors account for over 60% of hearing loss[41]. In this study, we developed a base editing tool, SchABE8e, by integrating nSchCas9 with the TadA-8e adenosine deaminase. This tool is characterized by its high editing efficiency, minimal off-target activity, a simple NNGR PAM requirement, and a broad editing window. Using the Anc80L65 capsid —known for its efficient transduction of hair cells—we delivered SchABE8e-sgRNA3 into the cochleae of neonatal *Pou4f3*$^{WT/Q113*}$ mice. This approach achieved a cDNA-level editing efficiency of 14.2 ± 2.5% for the pathogenic variant, preserving hearing function at levels comparable to WT mice. These results highlight the therapeutic potential of SchABE8e for C•G-to-T•A mutations. Due to its broad targeting range (NNGR PAM) and high activity, SchABE8e may also be applicable to other genetic forms of hearing loss.

Gene replacement therapy effectively compensates for defective proteins by delivering exogenous genes, thereby restoring hearing function, and has already entered clinical trials[17–19]. However, its therapeutic effect diminishes over time, requiring repeated administrations that impose a significant clinical burden. RNA editing technology

https://doi.org/10.1038/s41467-025-63613-w

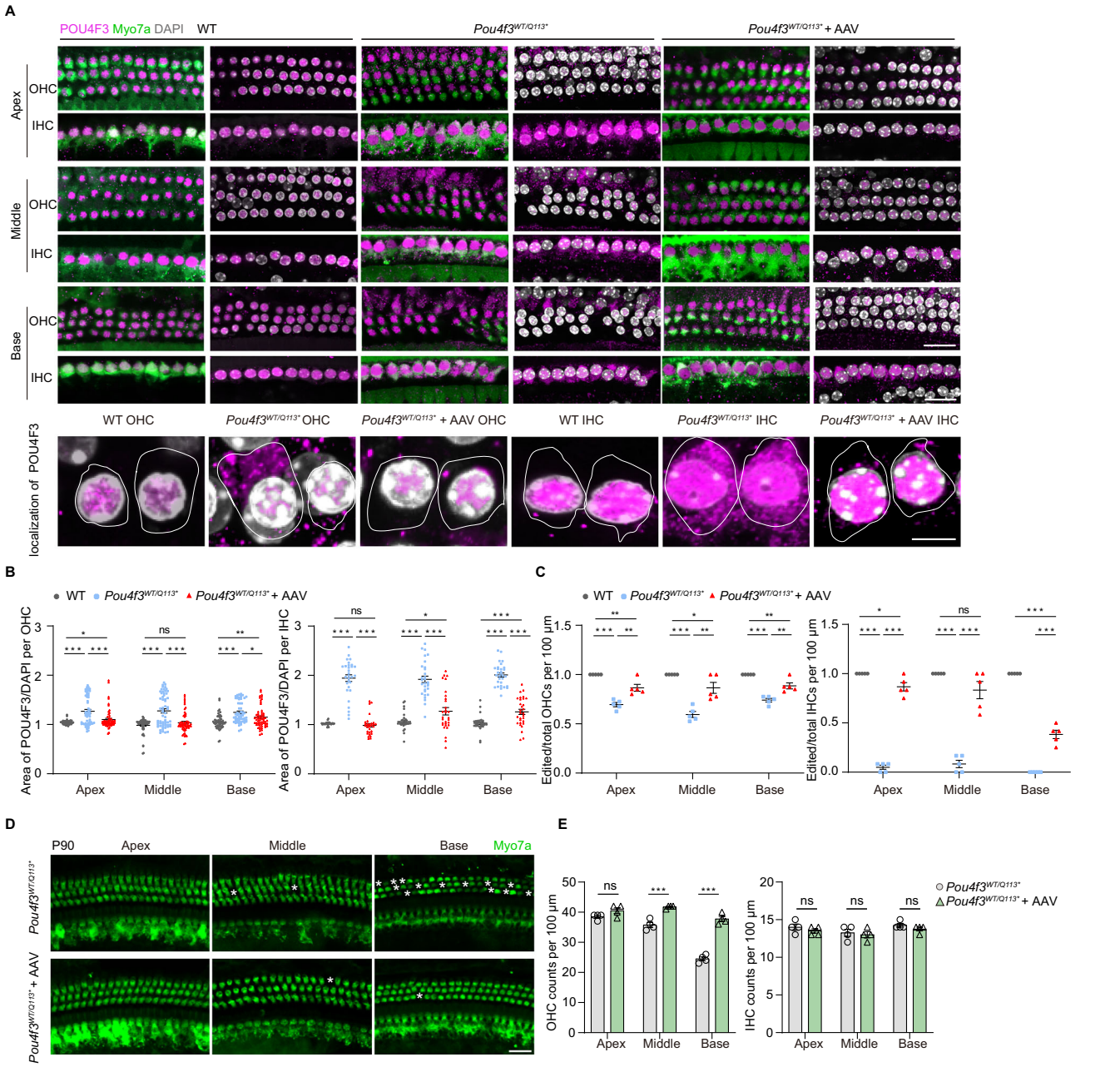

Fig. 5 | POU4F3 nuclear localization restoration and hair cell survival improvement in *Pou4f3*$^{WT/Q113*}$ mice post-injection. A Representative immunofluorescence images of POU4F3 localization in OHCs and IHCs across cochlear regions (apex, middle, and base) in WT, *Pou4f3*$^{WT/Q113*}$, and AAV-treated *Pou4f3*$^{WT/Q113*}$ mice, $n = 3$ independent experiments with similar results. Dashed circles represented the edges of hair cells. Myo7a (green): hair cell marker. Scale bar: 20 μm (top and middle rows), 5 μm (bottom row). **B** The proportion of POU4F3 protein signal overlapping the nuclear signal in the apical, middle, and basal turns of WT (gray), *Pou4f3*$^{WT/Q113*}$ (blue), and AAV-treated *Pou4f3*$^{WT/Q113*}$ mice (red) at P90. In OHCs ($n = 60$), WT vs *Pou4f3*$^{WT/Q113*}$, $p < 0.000001$ (apex, middle, and base), *Pou4f3*$^{WT/Q113*}$ vs *Pou4f3*$^{WT/Q113*}$ + AAV, $p = 0.000455$ (apex), $p = 0.000004$ (middle), $p = 0.014995$ (base); WT vs *Pou4f3*$^{WT/Q113*}$ + AAV, $p = 0.023242$ (apex), $p = 0.125571$ (middle), $p = 0.003470$ (base). In IHCs ($n = 30$), WT vs *Pou4f3*$^{WT/Q113*}$, $p < 0.000001$ (apex, middle, and base), *Pou4f3*$^{WT/Q113*}$ vs *Pou4f3*$^{WT/Q113*}$ + AAV, $p < 0.000001$ (apex, middle, and base); WT vs *Pou4f3*$^{WT/Q113*}$ + AAV, $p = 0.342315$ (apex), $p = 0.012933$ (middle), $p = 0.000280$ (base). **C** The proportion of edited/total OHCs or IHCs in 100 μm cochlear segments of the apical, middle, and basal turns for WT (gray), *Pou4f3*$^{WT/Q113*}$ (blue), and AAV-treated *Pou4f3*$^{WT/Q113*}$ mice (red) at P90 on enumeration of OHCs/IHCs with restored nuclear POU4F3 signals. In OHCs ($n = 5$), WT vs *Pou4f3*$^{WT/Q113*}$, $p < 0.000001$ (apex), $p = 0.000001$ (middle), $p < 0.000001$ (base); *Pou4f3*$^{WT/Q113*}$ vs *Pou4f3*$^{WT/Q113*}$ + AAV, $p = 0.003261$ (apex), $p = 0.002853$ (middle), $p = 0.003530$ (base); WT vs *Pou4f3*$^{WT/Q113*}$ + AAV, $p = 0.004828$ (apex), $p = 0.041546$ (middle), $p = 0.005185$ (base). In IHCs ($n = 5$), WT vs *Pou4f3*$^{WT/Q113*}$, $p < 0.000001$ (apex and middle); *Pou4f3*$^{WT/Q113*}$ vs *Pou4f3*$^{WT/Q113*}$ + AAV, $p < 0.000001$ (apex), $p = 0.000048$ (middle), $p = 0.000018$ (base); WT vs *Pou4f3*$^{WT/Q113*}$ + AAV, $p = 0.013850$ (apex), $p = 0.092971$ (middle), $p < 0.000001$ (base). **D** Representative immunofluorescence images of the cochleae in the apical, middle, and basal turns from untreated or AAV-treated *Pou4f3*$^{WT/Q113*}$ ears, $n = 4$ independent experiments with similar results. Scale bar, 20 μm. **E** Quantitative comparison of surviving OHCs and IHCs in the apical, middle, and basal turns from uninjected or AAV-injected *Pou4f3*$^{WT/Q113*}$ ears, OHC ($n = 4$), *Pou4f3*$^{WT/Q113*}$ vs *Pou4f3*$^{WT/Q113*}$ + AAV: $p = 0.113532$ (apex), $p = 0.000518$ (middle), $p = 0.000017$ (base); IHC ($n = 4$), *Pou4f3*$^{WT/Q113*}$ vs *Pou4f3*$^{WT/Q113*}$ + AAV, $p = 0.355918$ (apex), $p = 0.704853$ (middle), $p = 0.207031$ (base). Data in (**B**, **C**, **E**) are represented as mean ± SEM. Statistical significance was determined by two-tailed Student's *t*-tests ($^{*}p < 0.05$, $^{**}p < 0.01$, $^{***}p < 0.001$, ns no significant difference). Source data are provided as a Source data file.

https://doi.org/10.1038/s41467-025-63613-w

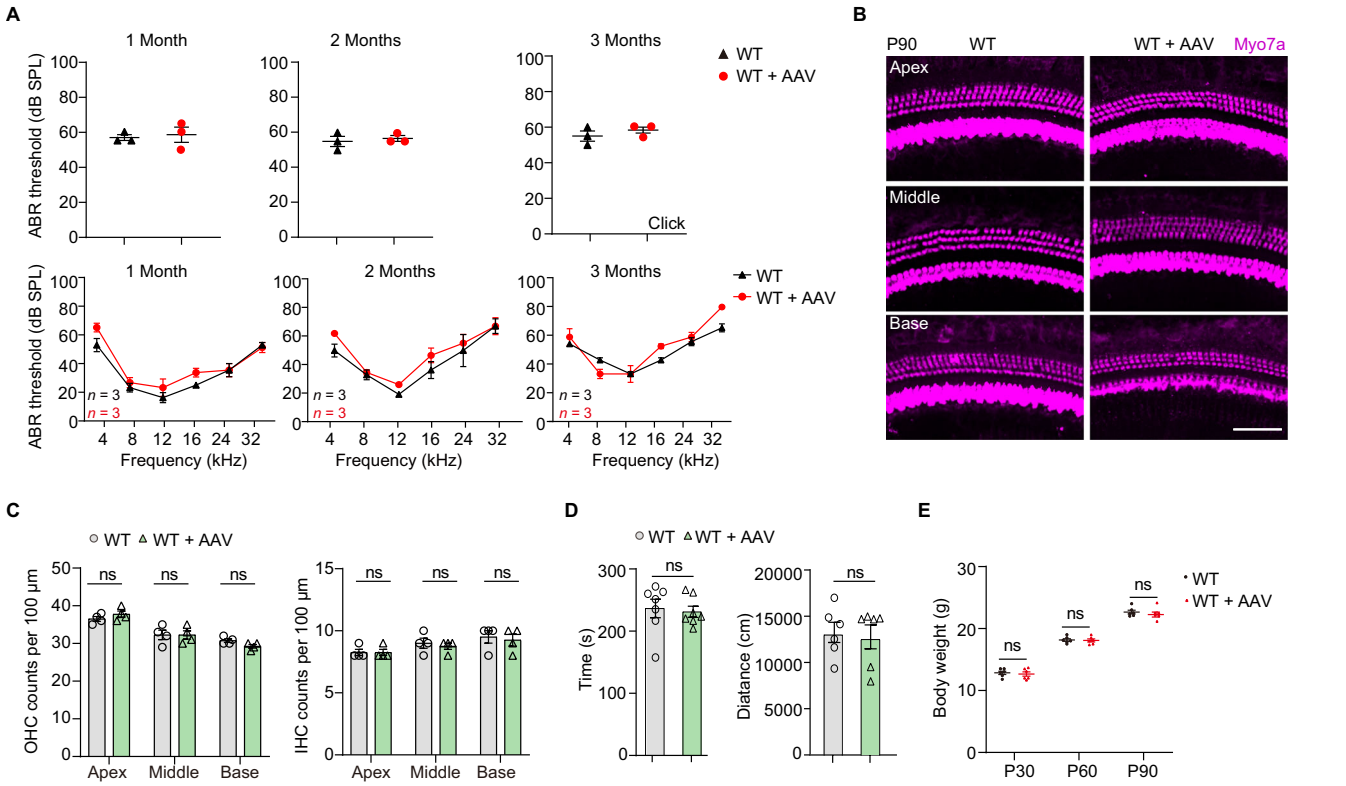

Fig. 6 | Therapeutic dual AAV-SchABE8e-sgRNA3 is safe in the inner ear. A Click ABR and TB-ABR thresholds at 1-, 2-, and 3-month post AAV injection. Neonatal WT mice (red, $n = 3$) were injected with the same dose of dual AAV-SchABE8e-sgRNA3 into the inner ear in the pharmacodynamic assay. Click ABR and TB-ABR were performed at 1-, 2-, and 3-month post-injection. **B** Representative immunofluorescence images of cochleae from WT and WT mice injected with dual AAV-SchABE8e-sgRNA3 at P90, $n = 4$ independent experiments with similar results. Myo7a (magenta): hair cell marker. Scale bar, 20 µm. **C** Cell counts comparison of OHCs and IHCs corresponding to (**B**), $n = 4$. **D** Behavior tests comparison between WT (black) and WT mice injected with dual AAV-SchABE8e-sgRNA3 (red) at P90. Left, $n = 7$, right, $n = 6$. **E** Body weight comparison between WT (black) and WT mice injected with dual AAV-SchABE8e-sgRNA3 (red), $n = 6$. Data in (**A**, **C**, **D**, **E**) are represented as mean ± SEM. Statistical significance was determined by two-tailed Student's *t*-tests (ns no significant difference). Source data are provided as a Source data file.

enables precise base modifications at the RNA level and has been used to restore hearing in deaf mice in studies by Xue et al. and Xiao et al.[42,43], However, this approach does not provide a permanent solution, as the edits are not heritable. CRISPR/Cas9 gene editing technology can replace target sequences through homologous recombination, but its utility is limited by low editing efficiency[44]. In contrast, base editing technology allows for the direct and effective correction of target bases at the DNA level and has been widely used in genetic disease treatment[45]. The ABE tools we developed exhibit broad targeting ranges. SchABE8e-sgRNA3 was selected as the optimal combination based on its editing efficiency (nearly 50%), high accuracy, low bystander editing, minimal indel formation, and safety profile. Although splitting SchABE8e into two components to form a dual-AAV system was necessary to bypass the AAV packaging capacity, this method successfully delivered the SchABE8e-sgRNA3 into the cochleae of *Pou4f3*$^{WT/Q113*}$ neonatal mice. Furthermore, tests on both endogenous targets and potential off-target sites for SchABE8e had demonstrated a broad editing window (protospacer positions 6-14), compatibility with simple NNGR PAM, high editing efficiency coupled with low off-target activity. These findings confirm that SchABE8e is a versatile and safe tool, providing valuable insights for research applications involving other C•G to T•A pathogenic mutations, including those related to deafness.

Although SchABE8e shows promise, we still need to address its ~6.2% bystander editing. There remains scope for further optimization. Replacement of its adenine deaminase with a more precise variant reduced bystander editing but also significantly decreased on-target editing efficiency. One alternative solution is to use more effective AAVs to reduce the therapeutic dose. Future efforts will focus on optimizing hair cell-specific serotypes and promoters to enhance the viral transduction efficiency.

In this study, we demonstrated that SchABE8e-mediated in situ DNA base editing significantly improved auditory function in *Pou4f3*$^{WT/Q113*}$ dominant deaf mice. We observed effective base editing of the pathogenic variant at the cDNA level 1 week post-injection. *Pou4f3*$^{WT/Q113*}$ mice exhibit late-onset, progressive hearing loss, beginning around P60. Accordingly, our study primarily focused on monitoring hearing function and quantifying hair cell survival from two months post-treatment onward. This design allows for a better understanding of the long-term effects of the treatment and the time course of hearing restoration. By 2 months post-treatment, the average Click-ABR threshold reached 60 dB, comparable to WT mice. *Pou4f3*$^{WT/Q113*}$ mice showed significant OHC degeneration at P90. Treated ears exhibited a significant preservation of OHCs, particularly in the apical and middle turns, aligning with the observed auditory improvements. Immunofluorescence analysis revealed that while untreated mice displayed cytoplasmic mislocalization of POU4F3, treated samples showed restored nuclear localization, confirming functional correction of the pathogenic variant. Remarkably, the therapeutic effect remained stable up to 4 months after treatment, confirming the long-term efficacy of SchABE8e-sgRNA3. However, this strategy was ineffective in homozygous mice due to irreversible hair cell loss prior to treatment.

Significant improvements were observed at low frequencies: 40 dB SPL at 8 kHz, 30 dB SPL at 12 kHz, and 40 dB SPL at 16 kHz. High-

frequency hearing also showed improvement, a 25 dB SPL difference persisted relative to WT mice. High-frequency hearing is primarily perceived by the basal turn hair cells. In *Pou4f3*$^{WT/Q113*}$ mice, the modest hearing improvement in high-frequency likely reflects low viral transduction efficiency within this cochlear region. Future studies should focus on enhancing transduction specifically in the basal turn to improve high-frequency hearing restoration.

Given the critical role of safety in clinical translation, results of nearly undetectable off-target editing in the cochlea are promising. Additionally, viral injection into WT mice did not affect auditory thresholds, hair cell counts, or morphology, demonstrating the safety and reliability of local SchABE8e therapy. Considering the Anc80L65 serotype can also transduce vestibular hair cells, behavioral tests are necessary and show no change. No significant difference in different indexes compared to controls addressed the comprehensive safety profiles of the whole inner ear.

Recently, Cui et al. achieved effective hearing restoration for up to 1.5 years in *Otof*$^{Q828*/Q828*}$ recessive deaf mice using NG-ABE7.10max, demonstrating the potential of ABEs for the stable treatment of inherited deafness[46]. In our study, current hearing tests in treated *Pou4f3*$^{WT/Q113*}$ mice extend to four months post-treatment. We plan to continue hearing assessment to explore the durability of this strategy in restoring hearing.

In summary, we developed SchABE8e, a pioneering base editor that achieved precise and effective treatment of *Pou4f3*$^{WT/Q113*}$ mice. Our findings lay a critical foundation for translational research in DFNA15, offering a therapeutic strategy through targeted correction of pathogenic mutations. The successful and near-complete restoration of auditory function in this model underscores the clinical promise of precision genome editing for treating human DFNA15.

Methods

Animals and ethics statement

The *Pou4f3*$^{WT/Q113*}$ point mutation mice used in this study were generated by introducing a c.337C > T mutation into C57BL/6J WT mice via CRISPR/Cas9. The *Pou4f3* (p.Q113*) mutation is located in exon 2 of mouse chromosome 18 (Gene ID: NM_138945.2), changing the WT codon sequence GCGGTACAT(CAG)GGCCTCGA to the mutant GCGGTACAT(TAG)GGCCTCGA. The mouse model was generated by Cyagen Biosciences.

All animal experiments were conducted using age-matched mice without sex-specific considerations and complied with the regulations of the ethics committee and animal welfare guidelines. All relevant operations on the experimental mice were approved by the ethics committee of Southeast University, with the approval number 20230216012. All mice were bred and maintained under specific pathogen-free (SPF) conditions in the animal facility of Southeast University, under a 12-h light/dark cycle with controlled temperature (20 ± 1 °C) and relative humidity (50 ± 5%).

Plasmids and cloning

This study utilized two main types of plasmids, namely tool plasmids and target plasmids. The tool plasmids were constructed by modifying the ABE8e plasmid (Addgene: #138489). Specifically, the nSpCas9 component was excised from the ABE8e plasmid via restriction enzyme digestion. Custom primers for nSha2Cas9, nSpeCas9, and nSchCas9 were synthesized by Sangon Biotech, and the target fragments were amplified by PCR. These fragments were then inserted into the plasmid using recombinase.

Subsequently, the modified plasmids served as vectors for further engineering. The TadA-8e component was removed by restriction enzyme digestion, and primers were designed to amplify TadA-8e-N108Q (Addgene: #194157) or TadA-8e-N108Q/L145T (Addgene: #194208). These fragments were inserted into the plasmid vector to generate a tool plasmid library. The elements and ABE tools protein sequence were provided in Supplementary Data 1.

The target plasmids were constructed using the U6-sgRNA-Scaffold-EF1α-EGFP plasmid as the backbone. A 21 bp oligonucleotide containing the target sequence was introduced at the *BbsI* restriction site using T4 DNA ligase. Following recombination, the plasmids were transformed into *Trans5α* competent cells and cultured at 37 °C for 16 h on bacterial culture plates. A single colony was selected from the liquid medium. Plasmid extraction was performed using a plasmid mini-prep kit (TIANGEN, #DP103), and the sequences were verified by Sanger sequencing.

Cell culture and stable cell line construction

HEK293T cells (Meisen, #CTCC-001-0188) were cultured in DMEM (Gibco, #8122093) supplemented with 10% fetal bovine serum (Vazyme, #F102) and 1% penicillin-streptomycin (Gibco, #15140122) at 37 °C, 90–95% humidity, and 5% CO_2. Cells were passaged at >90% confluency.

To generate a stable cell line harboring the mouse *Pou4f3*^{Q113*} mutation (c.337C > T), we designed primers flanking the around 260-bp target sequence (120 bp upstream/downstream of the mutation site) using NCBI Primer-Blast. The fragment was cloned into a lentiviral vector via recombination. Lentivirus was produced by transfecting HEK293T cells with a three-plasmid packaging system. Following an 8–10-h incubation, the culture medium was refreshed. Viral particles were harvested after 48 h, concentrated via ultracentrifugation, and cryopreserved at −20 °C.

For transduction, cells were seeded in six-well plates (30–50% confluency) and incubated with lentiviral supernatant. After 24 h, the medium was refreshed. Transduced cells (identified by red fluorescent protein expression (RFP)) were selected with puromycin (lentiviral vector markers: RFP and puromycin resistance). The *Pou4f3*^{Q113*} stable cell line was validated after sequential passaging.

Plasmid transfection and editing efficiency testing

For plasmid transfection, we used polyethyleneimine linear (PEI) (Yeasen, #40816ES02/03) at a 3:1 ratio (3 μL PEI: 1 μg plasmid). Cells were seeded in 24-well plates at optimized densities. Transfection was initiated at 60–70% confluency. Solution A (3 μL PEI + 50 μL DMEM) was mixed with Solution B (1 μg plasmid + 50 μL DMEM), incubated (15 min, RT), and added to cells. Following an 8–10-h incubation period, the spent medium was exchanged for fresh culture medium and changed daily until cells were collected for sorting at 72 h post-transfection. Editing validation assays of the ABE and targets used 1 μg total plasmid per cell (750 ng ABE plasmid, 250 ng sgRNA plasmid with EGFP for sorting). For SchABE8e variants testing, plasmids encoding N-terminal, C-terminal, and full-length constructs were 1:1:1 molar ratio.

GFP-based cell sorting was performed using a Fluorescence-activated cell sorter (BD FACSAria Fusion). For HEK293T cells, fluorescence gating was established using negative controls and GFP-positive control cells (Supplementary Fig. 7). GFP-expressing populations from transfected cells were collected and processed for genomic DNA extraction kit (TIANGEN, #DP304), followed by target-site PCR amplification and NGS (performed by Azenta).

NGS and data analysis

To assess on- and off-target editing efficiency, we amplified genomic regions of interest (~100 ng genomic DNA) with the following adapter-containing primers: forward (5′-GGAGTGAGTACGGTGTGC-3′) and reverse (5′-GAGTTGGATGCTGGATGG-3′). The amplicons were then subjected to a secondary PCR amplification with barcoded primers. Following library pooling, sequencing was performed on an Illumina HiSeq platform. For data analysis, we used BE-Analyzer (http://www.rgenome.net/be-analyzer) to precisely quantify both A-to-G conversion

and indel frequencies. Our analysis covered endogenous targets, dSpCas9 R-loop off-target sites, and SchCas9-dependent off-target sites (complete primer and target sequences: see Supplementary Data 2).

Off-target detection

To systematically evaluate Cas9-independent off-target editing, we first predicted potential sites (≤ 4 mismatches) using Benchling (https://www.benchling.com). Subsequently, the genomic coordinates of these sites were mapped against the NCBI human genome database. For each identified off-target locus, we designed specific primer pairs flanking 120 bp upstream and downstream regions using NCBI Primer-BLAST. These primers were then used for PCR amplification of target regions from flow-sorted cell genomic DNA. Finally, the amplified products were processed for NGS, and off-target editing efficiencies were quantified using BE-Analyzer to generate comprehensive off-target activity profiles (primer and target sequences provided in Supplementary Data 2).

WGS

We performed viral injection in neonatal heterozygous mice and collected the Organ of Corti tissues one week later for WGS. Given the limited quantity of cochlear sensory epithelia, we pooled tissues from three mice into a single composite sample (designated "treated"). As age-matched controls, we similarly pooled three cochlear sensory epithelia from uninjected mice (designated "untreated"). All WGS was performed by Azenta.

Genomic DNA (>200 μg) was sheared to 300–350 bp using Covaris, followed by end repair, A-tailing, and adapter ligation. Size-selected fragments were PCR-amplified with barcoded P5/P7 primers, purified, and quality-checked before 150 bp paired-end sequencing on Illumina HiSeq X Ten, NovaSeq, or MGI-2000 platforms.

For data analysis, raw reads were quality-checked, trimmed (Cutadapt v1.9.1; Q < 20), and filtered (>10% Ns discarded). Clean reads were aligned to mm10 (BWA 0.7.15), followed by germline variant calling (Sentieon/GATK HaplotypeCaller) and annotation (ANNOVAR).

Protein preparation and Western blotting

The secondary structure of nSchCas9 was predicted using PSIPRED Workbench (https://bioinf.cs.ucl.ac.uk/psipred). HEK293T cells were seeded in 6-well cell plates and transfected at 60-70% confluency. For transfection, 2 μg of full-length SchABE8e plasmid was used, while split versions (N- and C-terminal fragments) were mixed at a 1:1:1 molar ratio with the full-length plasmid. Culture medium was replaced 8–10 h post-transfection.

Protein extraction was performed 48 h post-transfection under ice-cold conditions: cells were washed twice with PBS, lysed in 200 μL RIPA buffer containing protease inhibitors, and centrifuged (13,400×*g*, 15 min, 4 °C) to collect the supernatant; protein extracts were then denatured with SDS at 95 °C for 10 min, aliquoted, and stored at −20 °C for subsequent analysis.

Electrophoresis and immunoblotting: 20 μL samples/well were loaded onto a 15-well precast gel (GenScript, #M00654; 100 V, 120 min). For protein transfer, PVDF membranes (Beyotime, #FFP19) were activated in methanol (Sangon, #A601617; 5 min). The transfer sandwich was performed in an ice-water bath (280 mA, 120 min). Membranes were then blocked (2 h, RT), briefly rinsed with 1×TBST (1–2 min, RT), and incubated with primary antibody: Rabbit anti-HA (Proteintech, #81290-1-RR; 1:2000), Rabbit anti-α-Tubulin (Proteintech, #81115-1-RR; 1:50000) at 4 °C. Membranes were washed with 1×TBST on a shaker (3 × 10 min, 50 rpm) the next day, followed by incubation with secondary antibody (Goat anti-rabbit IgG (H + L), Beyotime, #A0208; 1:1000; 1 h, RT). After three TBST washes, we detected signal using chemiluminescent substrate (NCM Biotech, #P0300) with a ChampChemi 610 imaging system. Western blot bands were quantified using ImageJ (Fiji, Inc.). Uncropped and unprocessed scans were added to the Source data file.

Mouse genomic DNA/RNA isolation and amplification

The Organ of Corti and cochlear epithelial tissue were dissected from euthanized mice and separately processed: genomic DNA was extracted using a commercial kit (TIANGEN, #DP304) for target region PCR amplification and NGS, while total RNA was extracted (Vazyme, #RC112), reverse transcribed (Thermo Fisher, #K1622), diluted 10-fold, and PCR-amplified for NGS analysis.

AAV production

We seeded HEK293T cells in 15 cm dishes (BIOFIL, #TCD000150). At 60–70% confluency, cells were transfected with AAV helper plasmids. The medium was replaced with medium containing 1% FBS after 10–12 h, and the cells and supernatant were collected 72 h post-transfection.

The cell pellet was resuspended with cell lysis buffer, and then the cell lysate underwent three freeze-thaw cycles to release the virus particles. The cell lysate was centrifuged (1800×*g*, 15 min), and the supernatant was collected. The supernatant was then loaded onto an iodixanol gradient ultracentrifugation column and centrifuged (400,000×*g*, 2 h, 4 °C). The virus particles were concentrated in the 40% iodixanol solution layer. The virus solution was then extracted using a syringe, diluted threefold with PBS, and transferred to a 100 kDa ultrafiltration tube. The virus was then concentrated and purified by centrifugation (1370×*g*, 30 min, 4 °C). The final purified virus was stored at −80 °C.

To determine the AAV titer, 1 μL virus was treated with 1 μL Dnase I (Thermo Fisher, #EN0525) to remove unpackaged DNA, and then proteinase K (Vazyme, #DE102) was added to release the viral genome. The treated virus was then diluted 100-fold and used for qPCR titer determination (using a CFX Opus 96 system).

Inner ear injection

P1–3 neonatal mice were anesthetized via ice immersion (2 min) and maintained on a cooled surface during surgery. The surgical area was disinfected with iodine, and a small incision was made in the skin behind the left ear, approximately 2 mm from the ear canal. Blunt dissection was used to separate the subcutaneous tissue, exposing the sternocleidomastoid muscle and facial nerve. The muscle and nerve were then retracted to expose the top of the cochlea and round window, and a 20 mm diameter glass needle was inserted to deliver 1.5 μL of virus solution. The needle was then withdrawn, and a small piece of muscle was used to block the entry point. The wound was closed with tissue adhesive, and the mouse recovered on a 37 °C heating pad before being returned to its mother.

Immunofluorescence labeling

Mice were euthanized, and the cochlear tissue was removed and cleaned of excess tissue in HBSS. A small hole was made on the top of the cochlea, and a microinjector was used to inject 4% paraformaldehyde (PFA) via the round window to wash out the blood and other impurities inside the cochlea. The cochlea was fixed overnight in 4% PFA, then washed twice with PBS and decalcified in 5 mM EDTA. After decalcification, the cochlear tissue was cut into sections. One microliter of Cell-Tak was placed on the center of a round glass slide and allowed to solidify, and the sections were carefully attached to the section to the slide in a four-well plate containing 1× PBS solution.

The PBS was removed from the four-well plate, and the cochlear sections were incubated in 1% PBST (PBS + 1% Triton X-100; 10 min, RT). The 1% PBST was removed, and the cochlear sections were immersed in blocking solution (0.05% PBST with 10% donkey serum; 1 h, RT). Seventy microliter primary antibody solution was added to each well and incubated overnight (Rabbit anti-Myo7a (Proteus

Bioscience, #25-6790; 1:1000), Mouse anti-POU4F3 (Santa Cruz, #81980; 1:400), Rat anti-HA (Roche, #11867423001; 1:200). Excess primary antibody was removed by washing with 1× PBS (3 × 5 min). Seventy microliters of corresponding secondary antibody solution was added to each well and incubated (1 h, RT; Donkey anti-Rabbit IgG (H + L), Alexa Fluor™ 555 (Invitrogen, #A-31572; 1:400), Donkey anti-Mouse IgG (H + L), Alexa Fluor™ 647 (Invitrogen, #A-31571; 1:400), Goat anti-Rat IgG (H + L), Alexa Fluor™ 488 (Invitrogen, #A-11006; 1:400) and DAPI (Solarbio, C0060; 1:1000). Excess secondary antibody was removed by washing with 1× PBS (3 × 5 min). The liquid was removed, and the round glass slide was placed on a slide holder for coverslipping. Ten microliters of mounting medium was evenly spread over the cochlea, and a round coverslip was placed on the cochlea-bearing slide, and the edges were sealed with nail polish, then imaged using a ZEISS LSM 900 confocal microscope after drying.

Hearing tests

Mice were anesthetized with a mixture of Zoletil 50 and xylazine (25 mg/10 mL), and injected intraperitoneally (10 μL/g body weight). Anesthetized mice were transferred to a soundproof box.

ABR: Electrodes were positioned as follows: (1) REF at the test ear pinna, (2) GND at the contralateral ear, and (3) CHAN at the cranial vertex. All electrodes were inserted subcutaneously with impedances maintained below 1 Ω. Acoustic stimuli were delivered through a closed-field speaker near the test ear canal via a silicone tube; DPOAE: a probe assembly containing a sensitive microphone and two miniature speakers was gently inserted into the external auditory canal. Two primary pure tones, f_1 and f_2, were presented simultaneously at an f_2/f_1 ratio of 1.22. The DPOAE threshold was defined as the lowest f_2 level at which the $2f_1 - f_2$ amplitude exceeded the mean noise floor (calculated from four adjacent frequency bins—two on each side of the $2f_1 - f_2$ frequency) by at least 3 dB SPL.

The TDTRZ6 system (Tucker-Davis Technologies) was used to assess auditory function. Post-procedure, mice were maintained under anesthesia on a 37 °C heating pad until complete recovery.

Behavioral assessments

To evaluate motor coordination, balance, and locomotor activity, mice underwent rotarod and open field tests under standardized conditions. In the rotarod test, mice were placed on an accelerating rod (10–40 rpm over 6 s, maintained at 40 rpm for 30 s). Each mouse received three trials with 5-min rest intervals. The latency to fall (time until dismount from the rod) was recorded as a key parameter of motor coordination.

For the open field test, mice were individually placed in a 50 × 50 × 40 cm arena for 30 min. Their movement was video-tracked, and the total walking distance was quantified to assess spontaneous locomotor activity.

Statistics and reproducibility

For in vitro experiments, all samples were analyzed with three independent biological replicates, following standard practices in the field. To enhance the robustness of therapeutic efficacy assessment, the sample size for in vivo experiments was increased ($n \geq 3$). Animal experiments were primarily divided into three groups: age-matched C57BL/6 J WT mice (serving as the positive control group), *Pou4f3*$^{WT/Q113*}$ mice treated with viral injection, and untreated *Pou4f3*$^{WT/Q113*}$ mice (serving as the negative control group). Within each group, mice of the same age were randomly assigned. No data were excluded. Detailed statistical analyses are provided in the respective figure legends. Sex-based differences were not considered in this study, as it was not relevant to the study objectives. Data are presented as mean ± SEM. Differences between groups were primarily analyzed using unpaired/paired two-tailed Student's *t*-tests or one-wayANOVA in GraphPad Prism 8 (GraphPad Software). Statistical significance was defined as $p < 0.05$.

Reporting summary

Further information on research design is available in the Nature Portfolio Reporting Summary linked to this article.

Data availability

Sequencing data (NGS/WGS) are available in the NCBI Sequence Read Archive (SRA) under accession code PRJNA1194950 without access restrictions. Source data are provided with this paper.

References

1. Brown, C. S. et al. Global hearing loss prevention. *Otolaryngol. Clin. North Am.* **51**, 575–592 (2018).
2. Jiang, L. et al. Advances in gene therapy hold promise for treating hereditary hearing loss. *Mol. Ther.* **31**, 934–950 (2023).
3. Stelma, F. & Bhutta, M. F. Non-syndromic hereditary sensorineural hearing loss: review of the genes involved. *J. Laryngol. Otol.* **128**, 13–21 (2014).
4. Aldè, M. et al. Autosomal dominant non-syndromic hearing loss (DFNA): a comprehensive narrative review. *Biomedicines* **11**, 1616 (2023).
5. Freitas, E. L. et al. Deletion of the entire POU4F3 gene in a familial case of autosomal dominant non-syndromic hearing loss. *Eur. J. Med. Genet.* **57**, 125–128 (2014).
6. Kim, H. J. et al. SNP linkage analysis and whole exome sequencing identify a novel POU4F3 mutation in autosomal dominant late-onset nonsyndromic hearing loss (DFNA15). *PLoS One* **8**, e79063 (2013).
7. Lee, H. K. et al. A novel frameshift mutation of POU4F3 gene associated with autosomal dominant non-syndromic hearing loss. *Biochem. Biophys. Res. Commun.* **396**, 626–630 (2010).
8. Vahava, O. et al. Mutation in transcription factor POU4F3 associated with inherited progressive hearing loss in humans. *Science* **279**, 1950–1954 (1998).
9. Li, Y. et al. Transcription factors expressed in mouse cochlear inner and outer hair cells. *PLoS One* **11**, e0151291 (2016).
10. Xiang, M. et al. Essential role of POU–domain factor Brn-3c in auditory and vestibular hair cell development. *Proc. Natl. Acad. Sci. USA* **94**, 9445–9450 (1997).
11. Alsina, B. et al. Regulation of the orphan nuclear receptor Nr2f2 by the DFNA15 deafness gene Pou4f3. *PLoS One* **9**, e112247 (2014).
12. Singh, S. et al. Highly variable hearing loss due to POU4F3 (c.37del) is revealed by longitudinal, frequency specific analyses. *Eur. J. Hum. Genet.* **31**, 815–823 (2023).
13. Zhang, C. et al. A novel nonsense mutation of POU4F3 gene causes autosomal dominant hearing loss. *Neural Plast.* **2016**, 1512831 (2016).
14. Pauw, R. J. et al. Audiometric characteristics of a Dutch family linked to DFNA15 with a novel mutation (p.L289F) in POU4F3. *Arch. Otolaryngol. Head. Neck Surg.* **134**, 294–300 (2008).
15. Anzalone et al. Genome editing with CRISPR-Cas nucleases, base editors, transposases and prime editors. *Nat. Biotechnol.* **38**, 824–844 (2020).
16. Zhang, L. et al. AAV-mediated gene therapy for hereditary deafness: progress and perspectives. *Adv. Sci.* **11**, e2402166 (2024).
17. Lv, J. et al. AAV1-hOTOF gene therapy for autosomal recessive deafness 9: a single-arm trial. *Lancet* **403**, 2317–2325 (2024).
18. Qi, J. et al. AAV-mediated gene therapy restores hearing in patients with DFNB9 deafness. *Adv. Sci.* **11**, e2306788 (2024).
19. Qi, J. et al. R. OTOF-related gene therapy: a new way but a long road ahead. *Lancet* **405**, 777–779 (2025).
20. Yeh, W. H. et al. In vivo base editing restores sensory transduction and transiently improves auditory function in a mouse model of recessive deafness. *Sci. Transl. Med.* **12**, eaay9101 (2020).
21. Peters, C. W. et al. Rescue of hearing by adenine base editing in a humanized mouse model of Usher syndrome type 1F. *Mol. Ther.* **31**, 2439–2453 (2023).

22. Gaudelli, N. M. et al. Programmable base editing of A*T to G*C in genomic DNA without DNA cleavage. *Nature* **551**, 464–471 (2017).
23. Wang, S. et al. Identification of SaCas9 orthologs containing a conserved serine residue that determines simple NNGG PAM recognition. *PLoS Biol.* **20**, e3001897 (2022).
24. Wang, S. et al. Compact SchCas9 recognizes the simple NNGR PAM. *Adv. Sci. (Weinh.)* **9**, e2104789 (2022).
25. Richter, M. F. et al. Phage-assisted evolution of an adenine base editor with improved Cas domain compatibility and activity. *Nat. Biotechnol.* **38**, 883–891 (2020).
26. Jeong, Y. K. et al. Adenine base editor engineering reduces editing of bystander cytosines. *Nat. Biotechnol.* **39**, 1426–1433 (2021).
27. Chen, L. et al. Engineering a precise adenine base editor with minimal bystander editing. *Nat. Chem. Biol.* **19**, 101–110 (2023).
28. Hwang, G. H. et al. Web-based design and analysis tools for CRISPR base editing. *BMC Bioinforma.* **19**, 542 (2018).
29. Thuronyi, B. W. et al. Continuous evolution of base editors with expanded target compatibility and improved activity. *Nat. Biotechnol.* **37**, 1070–1079 (2019).
30. Liu, Y. et al. Elimination of Cas9-dependent off-targeting of adenine base editor by using TALE to separately guide deaminase to target sites. *Cell Discov.* **8**, 28 (2022).
31. Doman, J. L. et al. Evaluation and minimization of Cas9-independent off-target DNA editing by cytosine base editors. *Nat. Biotechnol.* **38**, 620–628 (2020).
32. Yin, S. et al. Engineering of efficiency-enhanced Cas9 and base editors with improved gene therapy efficacies. *Mol. Ther.* **31**, 744–759 (2023).
33. Zhang, X. et al. Increasing the efficiency and targeting range of cytidine base editors through fusion of a single-stranded DNA-binding protein domain. *Nat. Cell Biol.* **22**, 740–750 (2020).
34. Wang, D., Tai, P. W. L. & Gao, G. Adeno-associated virus vector as a platform for gene therapy delivery. *Nat. Rev. Drug Discov.* **18**, 358–378 (2019).
35. Choi, J. H. et al. Optimization of AAV expression cassettes to improve packaging capacity and transgene expression in neurons. *Mol. Brain* **7**, 17 (2014).
36. Mingozzi, F. & High, K. A. Therapeutic in vivo gene transfer for genetic disease using AAV: progress and challenges. *Nat. Rev. Genet.* **12**, 341–355 (2011).
37. Landegger, L. D. et al. A synthetic AAV vector enables safe and efficient gene transfer to the mammalian inner ear. *Nat. Biotechnol.* **35**, 280–284 (2017).
38. Hudry, E. et al. Efficient gene transfer to the central nervous system by single-stranded Anc80L65. *Mol. Ther. Methods Clin. Dev.* **10**, 197–209 (2018).
39. Paterna, J. C. et al. Influence of promoter and WHV post-transcriptional regulatory element on AAV-mediated transgene expression in the rat brain. *Gene Ther.* **7**, 1304–1311 (2000).
40. Truong, D. J. et al. Development of an intein-mediated split-Cas9 system for gene therapy. *Nucleic Acids Res.* **43**, 6450–6458 (2015).
41. Alford, R. L. et al. American College of Medical Genetics and Genomics guideline for the clinical evaluation and etiologic diagnosis of hearing loss. *Genet. Med.* **16**, 347–355 (2014).
42. Xue, Y. et al. RNA base editing therapy cures hearing loss induced by OTOF gene mutation. *Mol. Ther.* **31**, 3520–3530 (2023).
43. Xiao, Q. et al. Rescue of autosomal dominant hearing loss by in vivo delivery of mini dCas13X-derived RNA base editor. *Sci. Transl. Med.* **14**, eabn0449 (2022).
44. Arnoult, N. et al. Regulation of DNA repair pathway choice in S and G2 phases by the NHEJ inhibitor CYREN. *Nature* **549**, 548–552 (2017).
45. Levy, J. M. et al. Cytosine and adenine base editing of the brain, liver, retina, heart and skeletal muscle of mice via adeno-associated viruses. *Nat. Biomed. Eng.* **4**, 97–110 (2020).
46. Cui, C. et al. A base editor for the long-term restoration of auditory function in mice with recessive profound deafness. *Nat. Biomed. Eng.* **9**, 40–56 (2025).

Acknowledgements

This work was supported by grants from the National Key Research and Development Program of China 2021YFA1101300 (R.C.), 2021YFA1101800 (R.C.), 2020YFA0112503 (R.C.), and 2020YFA0113600 (J.Q.); the National Natural Science Foundation of China 82330033 (R.C.), 82030029 (R.C.), 92468302 (R.C.), 92149304 (R.C.), 82371162 (J.Q.), U23A200440 (J.Q.), 82371161 (F.T.), 82192864 (H.Y.),82222017 (Z.H.), 82271183 (Z.H.), and 82401369 (L.Z.); the Key Program of Jiangsu Natural Science Foundation BF2025068 (R.C.) and BG2024037 (F.T. and Z.H.); the STI2030-Major Projects 2022ZD0205400 (J.Q.); the Taishan Scholars Project-Young Experts Program of Shandong Province tsqn202408320 (J.Q.); the Shandong Province Outstanding Youth Science Foundation ZR2024YQ049 (J.Q.); the Beijing Natural Science Foundation 7252089 (J.Q.); the Natural Science Foundation of Jiangsu Province BK20232007 (R.C.) and BK20241692 (L.Z.); the Shenzhen Science and Technology Program JCYJ20240813161801003 (R.C.); the Jiangsu Provincial Scientific Research Center of Applied Mathematics BK20233002 (R.C.); the 2022 Open Project Fund of Guangdong Academy of Medical Sciences YKY-KF202201 (R.C.); the Research Personnel Cultivation Program of Zhongda Hospital Southeast University CZXM-GSP-RC04 (F.T.); the China Postdoctoral Science Foundation 2024M750455 (L.Z.) and GZB20240145 (L.Z.); and Start-up Research Fund of Southeast University RF1028623028 (Z.H.).

Author contributions

R.C. conceived and supervised the study. M.W. designed, performed, and analyzed the in vitro experiments and generated figures. Z.Z. designed, performed, and analyzed the in vivo experiments and generated figures. X.W. and L.Z. assisted in the main experiments in vitro. X.C., N.L., Q.S., and Y.L. helped with the experiments in mice. M.W., Z.Z., Z.H., J.Q., and R.C. reviewed and edited the manuscript. F.T. and H.Y. provided technical support. All authors read and approved the final manuscript.

Competing interests

R.C., J.Q., M.W., Z.Z., F.T., X.W., L.Z., and X.C. have submitted a patent application to the China National Intellectual Property Administration pertaining to the application of SchABE8e inthe DFNA15 gene therapy aspect of this work (application number 202510477143.X; status: under review). The remaining authors declare no competing interests.

Additional information

Supplementary information The online version contains supplementary material available at https://doi.org/10.1038/s41467-025-63613-w.

Correspondence and requests for materials should be addressed to Hongbo Yang, Fangzhi Tan, Jieyu Qi or Renjie Chai.

Peer review information *Nature Communications* thanks the anonymous reviewers for their contribution to the peer review of this work. A peer review file is available.